Astron. Astrophys. 352, 257–265 (1999)

ASTRONOMY AND ASTROPHYSICS

Optical observations of three Galactic halo stars: evidence for cloudlets in intermediate- and high-velocity interstellar clouds

N. Lehner[1], K.R. Sembach[2], D.L. Lambert[3], R.S.I. Ryans[1], and F.P. Keenan[1]

[1] Department of Pure and Applied Physics, The Queen's University of Belfast, Belfast, BT7 1NN, Northern Ireland
[2] The John Hopkins University, Department of Physics and Astronomy, Bloomberg Center, 3400 N. Charles Street, Baltimore, MD 21218, USA
[3] Department of Astronomy, The University of Texas at Austin, Austin, TX 78712-1083, USA

Received 29 March 1999 / Accepted 12 October 1999

Abstract. Very high resolution ($R \sim 160000$) absorption line measurements of the interstellar Ca II K and Na I D lines and medium resolution ($R \sim 50000$) measurements of the interstellar Ti II (3384 Å) line towards three Galactic halo stars are presented. The data have signal-to-noise ratios of $\sim$ 90–240. The sightlines studied clearly show several intermediate-high velocity interstellar clouds with local standard of rest velocities in the range ~ -40 to $-110\,\mathrm{km\,s^{-1}}$. Two different methods have been used to analyze these data. Line profile fitting allows us to model multiple components for the different high-velocity clouds separated by only a few $\mathrm{km\,s^{-1}}$. The close proximity of the lines in velocity space indicates that the cloudlets are related. Conversion of the absorption profiles to apparent optical depth profiles also allows us to examine the column densities and their ratios as a function of velocity. Variations in $N(\mathrm{Ca\,II})/N(\mathrm{Na\,I})$, $N(\mathrm{Ca\,II})/N(\mathrm{Ti\,II})$ and $N(\mathrm{Ti\,II})/N(\mathrm{Na\,I})$ with cloud velocity are discussed.

Key words: ISM: general – ISM: clouds – ISM: structure – stars: early-type – Galaxy: halo

1. Introduction

High and intermediate velocity clouds (HVCs and IVCs[1], respectively) have been studied for many years through 21 cm H I observations. The radio data reveal that many IVCs/HVCs have a two-component velocity profile (e.g. Cram & Giovanelli 1976, Wakker & Schwarz 1991). However, the finite beam size of the 21 cm H I observations complicates the interpretation of the profiles (see the review by Wakker & van Woerden 1997). In principle, information about IVC/HVC velocity structure is available from optical and ultraviolet absorption lines seen in the spectrum of a star behind a IVC/HVC. To date, few sightlines containing IVCs/HVCs have been observed at spectral resolutions and signal-to-noise ratios sufficient to resolve the detailed structure within the absorption profiles. A notable exception is the HD 203664 sightline, which has an IVC detected by Little et al. (1994) at a Local Standard of Rest (LSR) velocity $v_{\mathrm{LSR}} \simeq 80\,\mathrm{km\,s^{-1}}$, using both H I and optical absorption line observations. Very high-resolution ($R \sim 200000$) optical spectroscopy of this sightline revealed the presence of multiple cloud components at $v_{\mathrm{LSR}} \simeq 70,\ 75,\ 80\,\mathrm{km\,s^{-1}}$ (Ryans et al. 1996). The narrow velocity spacing of these cloudlets suggests that they are related.

To better understand the nature of IVC/HVC velocity structure and to determine if other IVCs and HVCs are composed of similar cloudlets, we have undertaken an optical observing programme to examine several sightlines at high spectral resolution. The identification of cloudlet structure in IVCs/HVCs could have important implications for understanding the origin and evolution of IVCs and HVCs. Cloudlets within IVCs/HVCs have been suggested by Dyson & Hartquist (1983) as possible sites for star formation in the Galactic halo, which may account for some of the early-type stars observed at high Galactic latitudes. The identification of cloudlets within many IVCs/HVCs would lend support to this idea.

Previous observations ($R \sim 50000$) have revealed IVCs and HVC towards the stars HD 14633, HD 83206, and HD 93521 (Keenan et al. 1995, Ryans et al. 1997a, Ryans et al. 1997b). Absorption by intermediate and high velocity gas is visible in the Ca II K (3933.663 Å), Na I D (5889.951, 5895.924 Å) and Ti II (3383.768 Å) lines, but the observations were of insufficient resolution to resolve the IVC or HVC velocity structure. These three stars are bright enough to be re-investigated at very high spectral resolution ($R \sim 160000$), and we present here subsequent observations in the Ca II K and Na I D lines. These data allow us to resolve the IVC and HVC profiles into multiple components separated by only a few $\mathrm{km\,s^{-1}}$, and to conclude that cloudlet structure may be common to many IVCs and HVCs.

Send offprint requests to: Nicolas Lehner (N.Lehner@qub.ac.uk)

[1] For historical reasons, the peculiar velocity (values not permitted by the Galactic rotation) has been separated into two portions: $|v_{\mathrm{LSR}}| > 90\,\mathrm{km\,s^{-1}}$ (HVC) and $|v_{\mathrm{LSR}}| < 90\,\mathrm{km\,s^{-1}}$ (IVC). This division is arbitrary and may not reflect any real physical mechanisms. However, to avoid confusion with previous studies, we will keep this designation.

Table 1. Programme stars

Star	Sp	V (mag)	l ($^\circ$)	b ($^\circ$)	d (kpc)	z (kpc)	$v^{\rm a}_{\rm stellar}$ (km s^{-1})	$v \sin i$ (km s^{-1})
HD 14633	O8 V	7.5	140.78	-18.20	3.2	-1.0	-38	126
HD 83206	B2 V	8.6	167.70	46.93	1.5	1.1	25	< 6
HD 93521	O9 V	7.1	183.14	62.15	2.0	1.8	-13	400

[a] stellar radial velocity, in LSR.

2. Observations and data reduction

2.1. Programme stars

The principal properties of the stars are presented in Table 1, where z is the distance above or below the Galactic plane. These stars were first observed by us in a survey to determine the distances of the Intermediate Velocity Arch, Complex A, and Complex M (Keenan et al. 1995, Ryans et al. 1997a, Ryans et al. 1997b, unpublished data for HD 14633). Distances were estimated, in previous works, through a detailed spectroscopic parallax analysis. Atmospheric parameters (effective temperature and surface gravity of the star) were obtained from Strömgren *ubvy* photometry and/or spectroscopic data (see e.g., Ryans et al. 1997b for a more detailed discussion). Likely errors in the distance estimate are around 30%, due principally to errors in the determination of surface gravities. The stellar data for HD 14633 are from Hobbs (1983) and references therein; it is probably a runaway star ejected from the Perseus spiral arm. Ryans et al. (1997b) classified HD 83206 as a normal B-type star at $z = 1.2$ kpc. However, this star has also been observed by the Hipparcos astrometry mission, which has revealed a parallax of 3.86 ± 1.17 milliarcseconds, implying that this star may be an evolved object that lies at $z = 260$ pc. However, the 1σ error measurement is of the order of the measured values: the 1σ, 2σ, 3σ limits on the parallax distance are 370 pc, 660 pc, and 2860 pc. Thus, the spectroscopic distance lies at the $2 - 3\sigma$ limit of the Hipparcos distance estimate. Further analysis of the stellar spectrum (Lehner et al. 1999) using detailed non-LTE techniques seems to confirm that it is a main sequence B2-type star at a z-distance 1.1 kpc. HD 93521 has been the subject of considerable investigation and controversy concerning its nature, with evidence supporting both evolved and normal star hypotheses. However, Howarth & Reid (1993) have confirmed that HD 93521 is a normal Population I star at 1.8 kpc from the Galactic plane.

2.2. Observations

Spectra of the three stars were first obtained by our group during observing runs at the 4.2 m William Herschel Telescope during February 1993, December 1994, and February 1995. The Utrecht Echelle Spectrograph (UES) was used with the 79 lines per mm grating, and the Tek 1024×1024 CCD detector was employed for all observations. A number of different wavelength settings were used with UES, but in all cases spectra with near-complete coverage from 3000–5000 Å were obtained. Additional exposures were made to cover the interstellar Na I D lines. The instrumental configuration resulted in a resolution $R \sim 50000$. We present only the results for the Ti II absorption lines at this resolution since we re-observed the Na I and Ca II lines at higher resolution at McDonald Observatory. The observations of Ti II are sufficient to derive accurate column densities, since the observed 3384 Å line is weak and usually unsaturated (Stokes 1978). Ti II has an ionization potential of 13.6 eV, ensuring that it is the dominant ionization stage of Ti in H I regions (unlike Na I or Ca II).

Table 2. Signal-to-noise ratios

Star	Spectral Region	S/N
HD 14633	Ca II K	238
	Na I D	190
	Ti II	140
HD 83206	Ca II K	128
	Na I D	85
HD 93521	Ca II K	160
	Na I D	140
	Ti II	114

Observations of Na I and Ca II were carried out using the coudé spectrograph on the 2.7 m telescope at McDonald Observatory on 24–28 December 1996 with a Tektronix 2048×2048 CCD detector (Tull et al. 1995). Two wavelength settings per star were required to observe both the Ca II K and Na I D lines. This instrumental configuration resulted in a FWHM velocity resolution of ~ 1.9 km s^{-1} ($R \sim 160000$), which was determined from ThAr arc lines used for wavelength calibration.

For both sets of observations, short exposures of bright nearby stars were taken in the Na I region to act as telluric standards. Bias and quartz lamp flat field exposures were taken at the start and/or end of each night. ThAr exposures were interleaved with the stellar observations to allow wavelength calibration and to determine the spectral resolution of the data.

2.3. Data reduction

The raw CCD images were reduced to one dimensional spectra using the echelle reduction tools within the NOAO IRAF package (Morris & Privett 1995). The spectra were wavelength calibrated, and cross-correlation techniques were employed for multiple spectra of the same object to ensure that there was no shift between successive exposures. Spectra were normalized by fitting low-order polynomials to continuum areas. Images

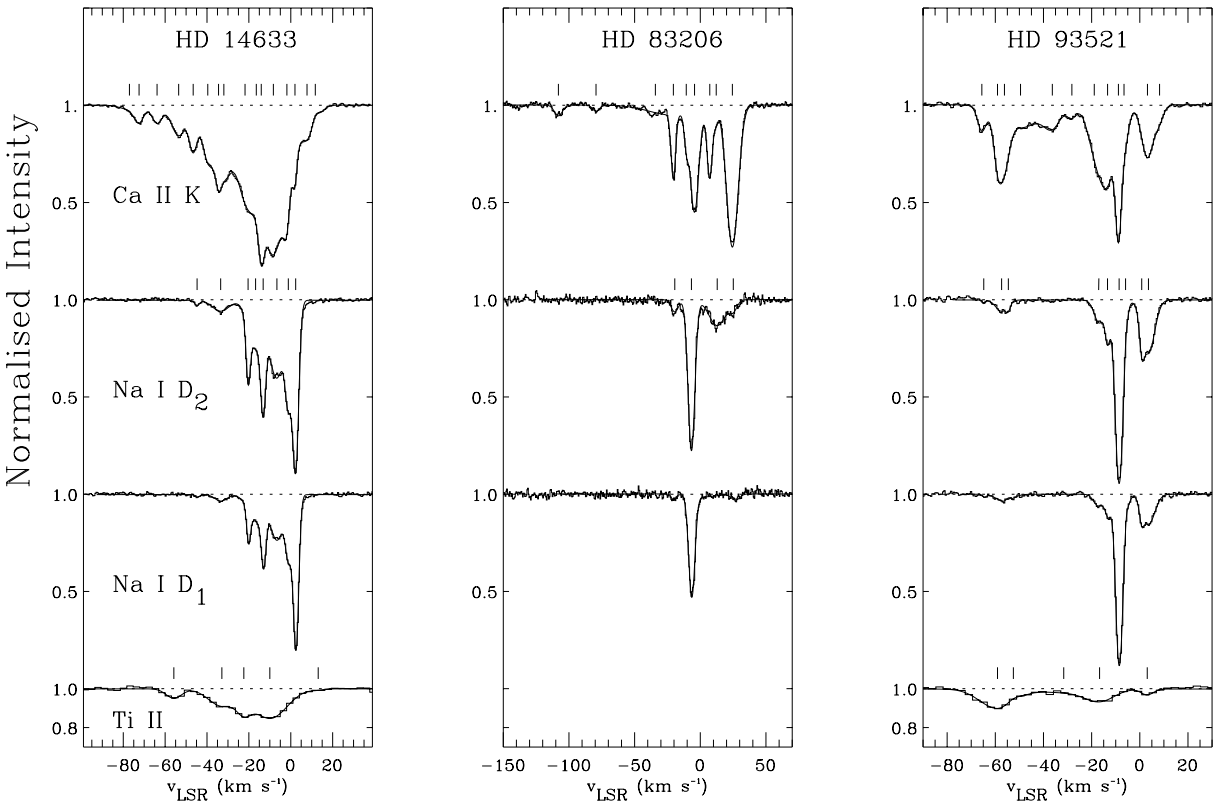

Fig. 1. Observed spectra (histograms) and their respective optimized fits (smooth lines) of Ca II K ($\lambda \sim 3933.66$ Å), Na I D ($\lambda \sim 5889.95, 5995.93$ Å) and Ti II ($\lambda \sim 3383.77$ Å) lines. The tick marks above the profiles denote the components found in the profile fits.

were then co-added, using weights determined by the continuum signal-to-noise levels. The Na I region spectra were corrected for telluric features using the atmospheric absorption observed towards the standard bright stars. Typical signal-to-noise ratios (S/N) of the co-added spectra are listed in Table 2. The spectra were shifted to the Dynamical LSR (Mihalas & Binney 1981), using corrections obtained from the STARLINK RV package (Wallace & Clayton 1996).

3. Analysis

3.1. Spectra and line profile fitting

The interstellar Ca II K, Na I D_1 and D_2, and Ti II features were first modelled using the optimized Gaussian fitting routines (ELFINP) in the STARLINK package DIPSO (Howarth et al. 1996) to obtain radial velocities, equivalent widths, and the full widths at half maximum intensity (FWHM$= 2\sqrt{\ln 2}\,b$, where $b^2 = 2kT/m + v_{turb}^2$). The complexity of the spectra (see Fig. 1) resulted in adoption of the following fitting method: (1) Before fitting the entire feature, we fit the spectrum component by component to give a reasonable initial estimate of the absorption properties. (2) Using these initial estimates, we allowed the fit parameters to vary and minimized the residuals between the fit and the data. Additional components were added only if they made a significant contribution to the quality of the final fit. We adopted the minimum number of components to adequately fit the observed profiles. (3) With this optimized fit, two of the three parameters ($v_{\rm LSR}$, b) were used in the multi-cloud model routine ISINP in DIPSO. These parameters were fixed, and the column density of each component was varied to obtain the best fit and errors for the normalized spectra. The magnitude of the instrumental broadening was described by a Gaussian with a width determined from the ThAr arc lines used for wavelength calibration. (We accounted for the intrinsic widths of the ThAr lines in this description.) The instrumental b-values were ~ 1.1 and 3.6 km s^{-1} for the McDonald and UES spectra, respectively. A singlet fitting routine was used to model the Ca II K line, and a doublet fitting routine was used for the Na I lines. The unresolved hyperfine splitting of the Na I lines was also taken into account when calculating the theoretical profiles using the routine ISINP. Since the routine ELFINP does not account for the hyperfine splitting, the b-values needed to be slightly adjusted to take the hyperfine splitting of the lines into account.

When we compared results from the Na I D_1 and D_2 lines, small differences in column density were found for strong local gas absorption between the D_1 and D_2 lines in the HD 14633 and HD 93521 spectra, which may indicate some saturation effects in the lines. However, the results were consistent within the limits of the errors (see below). Good agreement was found for the centroids of the different components, although small differences (but generally smaller than the resolution of the data) can be noticed between the Ca II and Na I components. The wavelengths and the oscillator strengths used were taken from the atomic data compilation given by Morton (1991).

Table 3. Cloud components for the three sightlines

Ion	$v_{\rm LSR}$ ($\rm km\,s^{-1}$)	E.W. (mÅ)	b ($\rm km\,s^{-1}$)	$\log(N)$ (cm^{-2})
		HD 83206		
Ca II K	-108.2 ± 0.2	5.6 ± 0.4	4.3 ± 0.3	10.85
	-79.8 ± 0.3	2.7 ± 0.4	4.3 ± 0.5	10.62
	-34.2 ± 0.6	11.5 ± 1.0	10.8 ± 1.2	11.15[a]
	-20.5 ± 0.1	18.6 ± 0.6	2.4 ± 0.1	11.52
	-10.7 ± 0.1	7.0 ± 0.8	2.2 ± 0.2	11.00
	-4.4 ± 0.1	55.5 ± 1.6	4.6 ± 0.1	11.99
	7.2 ± 0.1	24.6 ± 0.9	2.9 ± 0.1	11.58
	12.1 ± 0.2	2.9 ± 0.5	1.9 ± 0.2	10.53
	24.4 ± 0.1	106.2 ± 0.7	6.3 ± 0.1	12.27
Na I D_2	-108	< 0.5	...	< 9.4[b]
	-80	< 0.5	...	< 9.4[b]
	-34	< 1.3	...	< 9.8[b]
	-19.4 ± 0.5	8.5 ± 1.4	3.9 ± 1.0	10.56
	-6.7 ± 0.1	99.7 ± 0.9	3.7 ± 0.1	11.94
	12.9 ± 0.3	40.8 ± 2.2	8.8 ± 0.6	11.27
	25.1 ± 0.5	6.9 ± 1.7	4.1 ± 0.8	10.70
		HD 93521		
Ca II K	-65.6 ± 0.1	7.0 ± 0.8	2.5 ± 0.2	10.98
	-59.1 ± 0.4	12.6 ± 6.5	2.5 ± 0.2	11.24
	-56.2 ± 0.8	15.6 ± 7.2	2.9 ± 0.5	11.42
	-49.5 ± 0.9	31.3 ± 3.1	11.4 ± 1.1	11.57
	-36.3 ± 0.2	10.7 ± 1.8	4.7 ± 0.4	11.14
	-28.2 ± 0.2	4.0 ± 0.5	2.8 ± 0.4	10.68
	-18.9 ± 0.1	18.9 ± 0.9	4.5 ± 0.3	11.35
	-13.4 ± 0.1	42.9 ± 1.9	4.8 ± 0.2	11.80
	-8.9 ± 0.1	17.8 ± 2.0	1.7 ± 0.1	11.72
	-6.5 ± 0.3	11.9 ± 2.1	2.7 ± 0.2	10.90
	3.2 ± 0.1	22.2 ± 0.9	3.5 ± 0.1	11.48
	8.2 ± 0.3	4.2 ± 0.9	2.5 ± 0.3	10.60
Na I D_2	-64.8 ± 0.7	0.7 ± 0.3	1.1 ± 0.8	9.72
	-57.4 ± 0.7	6.9 ± 0.9	3.4 ± 0.7	10.55
	-54.6 ± 0.5	1.4 ± 0.7	1.2 ± 0.5	10.10
	-50	< 0.6	...	< 9.5[b]
	-36	< 0.6	...	< 9.4[b]
	-28	< 0.7	...	< 9.6[b]
	-17.1 ± 0.4	12.5 ± 1.1	2.6 ± 0.4	10.70
	-13.4 ± 0.1	8.8 ± 1.0	1.7 ± 0.1	10.85
	-8.6 ± 0.1	79.5 ± 0.7	1.3 ± 0.1	12.15
	-5.9 ± 0.2	1.1 ± 0.4	1.2 ± 0.2	10.20
	0.8 ± 0.2	6.6 ± 0.9	1.1 ± 0.2	10.60
	3.5 ± 0.2	35.2 ± 1.2	3.7 ± 0.2	11.37
Ti II	-59.1 ± 1.4	20.1 ± 3.0	10.0 ± 1.1	11.80
	-52.5 ± 1.5	1.3 ± 1.8	3.6 ± 2.2	10.30
	-31.6 ± 10.6	5.3 ± 3.7	14.5 ± 7.9	11.20
	-16.7 ± 1.3	10.2 ± 3.8	8.5 ± 1.5	11.50
	3.1 ± 0.8	2.1 ± 0.6	3.6 ± 1.0	10.95
		HD 14633		
Ca II K	-77.0 ± 2.9	3.2 ± 1.7	6.4 ± 2.2	10.61
	-72.5 ± 0.3	6.1 ± 2.0	3.2 ± 0.6	10.87
	-63.8 ± 0.1	7.5 ± 0.5	3.5 ± 0.3	10.95
	-53.5 ± 0.1	17.9 ± 1.0	4.9 ± 0.3	11.35
	-46.6 ± 0.1	13.0 ± 1.0	2.7 ± 0.1	11.27
	-39.6 ± 0.1	24.9 ± 2.0	4.2 ± 0.2	11.47
	-34.5 ± 0.2	4.7 ± 2.5	1.9 ± 0.4	11.00
	-32.0 ± 1.0	43.5 ± 8.8	5.4 ± 1.0	11.80
	-21.8 ± 1.7	60.1 ± 9.7	5.9 ± 0.7	11.89
	-16.5 ± 1.1	28.0 ± 14.8	4.3 ± 0.6	11.39
	-14.1 ± 0.1	8.9 ± 0.4	1.9 ± 0.1	11.56
	-8.3 ± 0.1	147.9 ± 8.5	8.3 ± 0.5	12.49
	-1.8 ± 0.1	12.5 ± 1.8	2.3 ± 0.1	11.23
	2.0 ± 0.1	6.1 ± 0.6	1.5 ± 0.1	10.75
	7.8 ± 0.5	22.5 ± 2.0	5.9 ± 0.3	11.25
	11.7 ± 0.1	2.5 ± 0.6	2.1 ± 0.2	10.30
Na I D_2	-75	< 0.5	...	< 9.3[b]
	-64	< 0.5	...	< 9.4[b]
	-53	< 0.5	...	< 9.4[b]
	-44.8 ± 0.2	1.5 ± 0.3	1.6 ± 0.4	10.10
	-33.5 ± 0.2	11.0 ± 0.6	5.6 ± 0.4	10.78
	-20.4 ± 0.1	14.0 ± 0.8	1.4 ± 0.1	11.12
	-16.8 ± 0.5	42.7 ± 4.0	5.1 ± 0.4	11.34
	-13.2 ± 0.1	22.1 ± 1.5	1.7 ± 0.1	11.90
	-6.6 ± 0.2	70.3 ± 6.9	5.1 ± 0.5	11.37
	-1.2 ± 0.1	29.4 ± 4.7	2.1 ± 0.2	11.63
	2.3 ± 0.1	61.3 ± 1.5	2.1 ± 0.1	11.30
Ti II	-55.8 ± 0.7	5.1 ± 0.7	5.2 ± 0.8	11.22
	-32.9 ± 1.6	16.1 ± 3.6	9.2 ± 1.9	11.70
	-22.4 ± 0.8	7.1 ± 4.4	4.8 ± 1.3	11.40
	-10.0 ± 0.9	35.1 ± 3.7	11.5 ± 1.2	12.05
	13.1 ± 6.9	0.5 ± 0.7	4.4 ± 6.9	10.25

[a] Component is a possible blend of narrower components centered near $-34\,\rm km\,s^{-1}$.
[b] No feature present. Upper limit is 3σ estimate.

Table 3 summarizes the results of the fitting process, and Fig. 1 shows the fits to the different profiles. Approximate 1σ fitting uncertainties are also shown in this table for the derived parameters $v_{\rm LSR}$, b, and equivalent widths. Errors in continuum placement can be particularly important for weak lines, such as those produced by the IVCs and HVC observed. A straightforward method to estimate this error is to take the RMS noise variation in the continuum and calculate the error on the equivalent width incurred by raising or lowering the entire continuum by an amount equal to $\sim +/-0.2$ times this RMS value (see e.g. Sembach & Savage 1992). Continuum errors on the equivalent width measurements were less than 0.4 mÅ in all cases, and less than 0.1 mÅ in cases where the S/N levels were very high. The errors listed in Table 3 do not include contributions from background uncertainties, though these are also expected to be small ($< 5\%$). Thus, these errors are principally dominated by the statistical errors. Finally, when the centroids and b-values are fixed, the column densities do not vary by more than ± 0.05–0.20 dex.

Table 4. Comparison of the total equivalent widths and column densities towards HD 14633, HD 83206 and HD 93521 from previous work with our estimates from the fitting procedure described in the text (denoted Fitting) and from the apparent optical depth method (denoted AODM) with no saturation correction applied.

	Ca II K		Na I D_2		Ti II	
	N (10^{11} cm^{-2})	EW (mÅ)	N (10^{11} cm^{-2})	EW (mÅ)	N (10^{11} cm^{-2})	EW (mÅ)
HD 14633						
Fitting	65.4	409	20.8	164	20.6	64
AODM	65.0	–	19.4	–	20.4	–
Previous Work [a]	62.2	397	18.9	178	21.2	68
HD 93521						
Fitting	28.9	199	15.9	153	12.2	40
AODM	27.7	–	12.5	–	13.0	–
Previous Work [b]	28.4, 24.8	–, 193	24.9, >24.0[c]	–,140	11.3, –	–
HD 83206						
Fitting	39.2	213	11.4	76.1	–	–
AODM	38.4	–	12.3	–	–	–

[a] Hobbs (1983).
[b] Spitzer & Fitzpatrick (1993), Welty et al. (1996) (Ca II K) and Hobbs (1978) (Na I).
[c] Results are from Na I D_1 line.

Several conclusions can be drawn from a comparison of the profiles and the profile fitting process: (1) Ca II has a larger velocity extent than Na I. This result is not unexpected, since it is typical for low density sightlines (Sembach & Danks 1994). (2) Ti II has a velocity extent comparable to that of Ca II. However, some component structure is less pronounced in the Ti II profiles. Some high velocity components (< -60 km s^{-1}) towards HD 93521 and HD 14633 are not observed in Ti II. This may be due in part to the lower resolution and S/N of the Ti II data. (3) Owing to large $v \sin i$ and early spectral type (see Table 1) for HD 14633 and HD 93521, no interference by stellar absorption lines is either expected or seen in Fig. 1. However, the spectra of HD 83206 contain a narrow absorption line at the stellar radial velocity of ~ 25 km s^{-1} having a width consistent with the low $v \sin i$ of the star (< 6 km s^{-1}). (4) IVC component at -65, -59, -56 km s^{-1} seen towards the star HD 93521 probe the cloud IV6 defined by Kuntz & Danly (1996). HD 83206 lies between the complex M and A (Fig. 1 in Wakker & van Woerden 1997), but in particular just off the HVC complex M which has velocities ~ -100 km s^{-1}.

The total column densities and equivalent widths derived from our data are in good agreement with previous observations of these sightlines (see Table 4). Results for HD 93521 can be directly compared with results from Welty et al. (1996) for the Ca II K line. Their data are of slightly higher spectral resolution but lower S/N. The same number of components is found, and there is a good correlation between the component centroids in the two studies. The total column densities are similar, but some differences can be found in the individual component N and b values. This gives some indication of the subjectivity of the profile fitting process. Spitzer & Fitzpatrick (1993) made an extensive study of the velocity structure towards HD 93521. Their results are also summarized in Table 4. There is similar good agreement between our results and those of Hobbs (1983) for the HD 14663 sight line, but the higher quality of our data reveals a larger number of components.

3.2. The apparent optical depth method

Profile fitting involves several important assumptions, such as an estimate of the significance of each component, the approximate values of the component parameters (i.e., initial guesses), and description of component velocities by a Maxwellian velocity distribution. In this section, we use an alternate approach to analyze the profiles – the apparent optical depth method described by Savage & Sembach (1991). This method is particularly well-suited for use on very high resolution data, and converts absorption line data into profiles of column density per unit velocity. It makes no a priori assumption about the functional form of the velocity distribution. To check for unresolved saturated structure, at least two absorption lines of a given species which differ in the product $f\lambda$, (where f is the oscillator strength), must be observed. The apparent optical depth is defined as $\tau_a = -\ln[I_{\rm obs}(v)]$, where $I_{\rm obs}$ is the normalized observed intensity, which is the convolution of the intrinsic spectrum and the instrumental spectral spread function. The apparent column density profile $N_a(v)$ (in cm^{-2} (km s^{-1})$^{-1}$) is

$$N_a(v) = -3.768 \times 10^{14} \frac{\ln[I_{\rm obs}(v)]}{f\lambda(\text{Å})} \,. \quad (1)$$

The apparent column density profile is a valid, blurred representation of the true column density profile, $N(v)$, if the profiles from two or more lines differing in $f\lambda$ agree at the same velocity. Otherwise, a correction for unresolved saturated structure may be necessary (see Savage & Sembach 1991 and Jenkins 1996

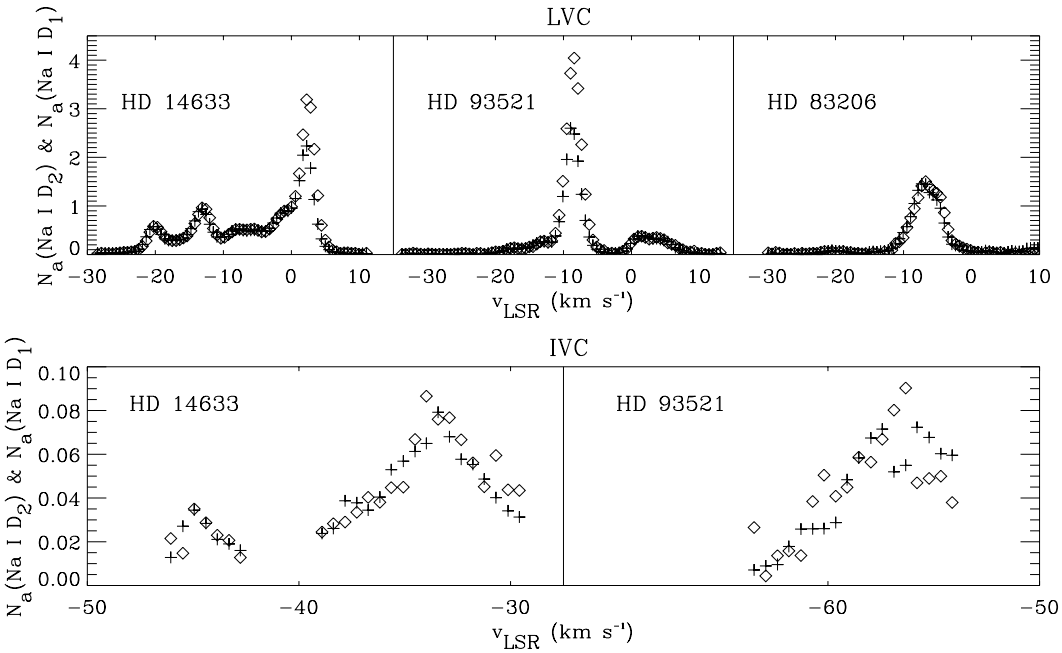

Fig. 2. Profiles of apparent column density of Na I D_1 ($\diamond$) and D_2 ($+$) in units of 10^{11} cm^{-2} (km s^{-1})$^{-1}$ versus $v_{\rm LSR}$ (LVC stands for Low Velocity Cloud)

for detailed discussions). A direct integration of the apparent column density profiles,

$$N_a = \int N_a(v)dv\,, \qquad (2)$$

yields the total column density of the line if there is no unresolved saturated structure present. Doublet Na I D lines are ideal for such investigations.

Fig. 2 shows the apparent column density profiles for the two Na I D lines observed towards each star. Some unresolved saturated structure is observed in the low velocity absorption (as was inferred using the profile fitting method) when $N_a \gtrsim 10^{11}$ cm^{-2} (km s^{-1})$^{-1}$, but not at lower column densities. IVC and HVC are not observed towards HD 83206 in the Na I D lines. Towards HD 14633, the IVC profiles agree relatively well for the two lines. The agreement is less obvious towards HD 93521, due to the smaller S/N ratio and the lower strength of the IVC Na I D lines. Since our primary goal in this paper is to study the IVC and HVC gas, we have not corrected the low velocity gas for saturation effects. (This explains most of the differences between our results and previous determinations of the total column density for Na I towards HD 93521, see Table 4.) The general good agreement between the $N_a(v)$ profiles for the Na I lines towards each star gives us reason to believe that the Ca II K line also does not contain any unresolved saturated structure, since the observed IVC Ca II lines have apparent optical depths less than those of Na I, where unresolved saturated structure is present. Ca II traces both the cloud core structure seen in Na I as well as more pervasive diffuse gas, which is generally weak compared to the cloud core absorption. The core absorption regions traced by Ca II also tend to be a bit broader and weaker in their cores since dust depletion in these regions limits the Ca abundance in the gas. Similar comments apply to the Ti II line. The resolution of the UES data ($b_{\rm inst} \sim 3.5$ km s^{-1}) is lower than the McDonald data, but the Ti II IVC absorption is considerably weaker than the Ca II absorption (see Table 4).

In Table 4 we present the column densities obtained using Eq. 1. Integration of the $N_a(v)$ profiles yields column densities similar to the profile fitting method once saturation corrections for the low velocity line cores are taken into account.

4. Results and discussion

4.1. Column density ratios

In Fig. 3, we plot the $N({\rm Ca\,II})/N({\rm Na\,I})$ ratios versus LSR velocity, which follow directly from Eqs. 1 and 2 using the McDonald data, while in Fig. 4 we present $N({\rm Ca\,II})/N({\rm Ti\,II})$ and $N({\rm Ti\,II})/N({\rm Na\,I})$ ratios versus LSR velocity from the UES and McDonald data. Since the spectral resolution of the UES data is lower than that of McDonald, we re-binned the Ca II and Na I results in order to obtain the same resolution, and then, as previously, Eq. 1 was directly applied.

From these figures, several conclusions can be drawn:

(1) The Ca II/Na I ratio depends strongly on the LSR velocity (the Routly-Spitzer (1952) effect). For these sightlines two typical velocity ranges can be defined:

(i) when $|v_{\rm LSR}| < 20$ km s^{-1}:

$0.5 \lesssim N_a({\rm Ca\,II})/N_a({\rm Na\,I}) \lesssim 10.0$;

$0.1 \lesssim N_a({\rm Ti\,II})/N_a({\rm Na\,I}) \lesssim 2.0$

(ii) when $|v_{\rm LSR}| > 20$ km s^{-1}:

$10.0 \lesssim N_a({\rm Ca\,II})/N_a({\rm Na\,I}) \lesssim 65.0$;

$3.0 \lesssim N_a({\rm Ti\,II})/N_a({\rm Na\,I}) \lesssim 35.0$.

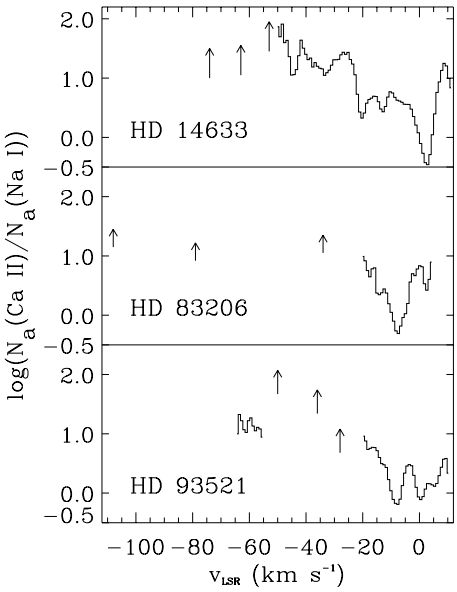

Fig. 3. $N_a(\mathrm{Ca\,II})/N_a(\mathrm{Na\,I})$ line ratio versus LSR velocities for the three stars under study. Arrows indicate lower limit of this ratio obtained from the upper limit estimate at 3σ of Na I D_2 column density (see Table 3)

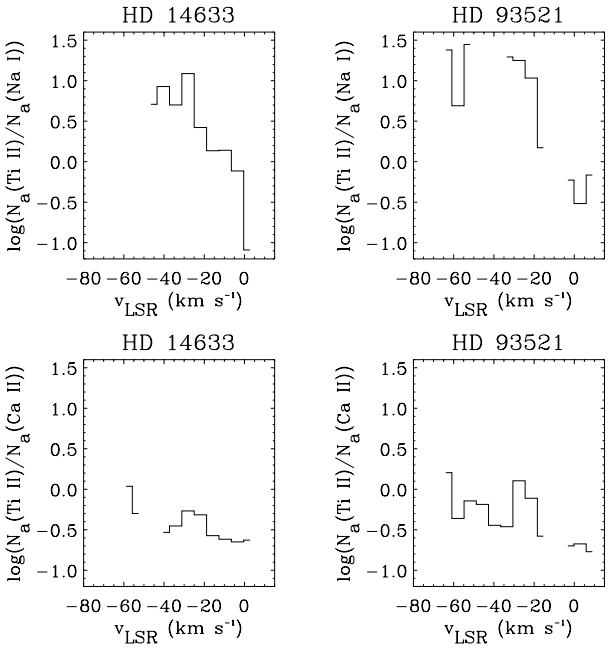

Fig. 4. $N_a(\mathrm{Ca\,II})/N_a(\mathrm{Ti\,II})$ and $N_a(\mathrm{Ti\,II})/N_a(\mathrm{Na\,I})$ ratio versus LSR velocities for HD 14633 and HD 93521

These values are consistent with previous studies (see e.g., Sembach & Danks 1994 and references therein). Two principal mechanisms are responsible for changes in the column density ratios with velocity, namely preferential ionization of Na I compared to Ca II or Ti II and/or liberation of Ca and Ti from dust grains in the IVC and HVC gas. From previous theoretical and observational studies (see Sembach & Danks 1994 and references therein), it is now believed that the major contribution to the changes in Ca II and Ti II to Na I ratio occurs as a result of the highly variable gas phase abundance. Values of $N_a(\mathrm{Ca\,II})/N_a(\mathrm{Na\,I})$ greater than 10, and as large as 65, for the IVC and HVC, occur under conditions where the grains are partly destroyed, or entirely destroyed for values greater than 50 (Hobbs 1983). The destruction of grains by shocks and the subsequent release of calcium and titanium into the gas phase provides a simple explanation of the increased abundance of Ca II and Ti II relative to Na I in the IVCs.

(2) Fig. 4 shows that the $N_a(\mathrm{Ti\,II})/N_a(\mathrm{Ca\,II})$ ratio varies less from cloud to cloud compared to change in $N_a(\mathrm{Ti\,II})/N_a(\mathrm{Na\,I})$ over similar velocity intervals. Hobbs (1983) studied extensively the sightline towards HD 14633, and found that the $N(\mathrm{Ti\,II})/N(\mathrm{Ca\,II})$ ratio varies between 0.2 and 1.0 with LSR velocity. With the higher quality of our data and the method used which gives a larger sample than Hobbs, this result is confirmed since we find a very similar range between 0.2 and 1.1. In the case of HD 93521, variation is slightly larger, between 0.2 and 1.6. From Hobbs (1983), the column density ratio is given by $N(\mathrm{Ca\,II})/N(\mathrm{Ti\,II}) \propto \delta(\mathrm{Ca})/\delta(\mathrm{Ti})/(1+\beta(\mathrm{Ca})/n_e)$, where $\delta(x)$ is the gas-phase depletion factor, and $\beta(\mathrm{Ca})/n_e$ is the calcium ionization balance. Previous studies (Stokes 1978, Albert et al. 1993, Welsh et al. 1997) have shown that Ca II and Ti II column densities are correlated, implying that these ions are controlled by the same physical mechanisms. Thus, although overall Ca II and Ti II depletion factors vary widely from cloud to cloud, their ratio must be relatively constant. Therefore, the variation observed in the bottom panel of Fig. 4 is probably due mainly to variation in the calcium ionization balance.

Finally, in a study of the Milky Way halo gas, Albert et al. (1993) found an average total integrated column density ratio $N(\mathrm{Ca\,II})/N(\mathrm{Ti\,II})$ of ~ 0.4, while Welsh et al. (1997) found ~ 0.29 for disk gas. This ratio is 0.31 for HD 14633 and 0.42 for HD 93521. HD 14633 is at much lower galactic latitude than HD 93521, and thus our results appear to be consistent with these previous studies.

4.2. Evidence for cloudlets in IVCs and HVCs

Ryans et al. (1996) found multiple cloud components in the IVC Ca II and Na I absorption lines towards the halo star HD 203664. This was a clear case in which the higher velocity gas showed cloudlet substructure. Our profile fitting results (see Table 3 and Fig. 1) clearly indicate that we detect subcomponents in the IVC gas towards HD 14633 ($v_{\mathrm{LSR}} = -77.0, -72.5, -63.8, -53.5; -46.6, -39.6, -34.5, -32.0\,\mathrm{km\,s^{-1}}$ for the Ca II K line and $-44.8, -33.5$ for Na I line) and HD 93521 ($v_{\mathrm{LSR}} = -65.6, -59.1, -56.2, -49.5\,\mathrm{km\,s^{-1}}$ for the Ca II K line and $-64.8, -57.4, -54.6\,\mathrm{km\,s^{-1}}$ for Na I line). There may be a small systematic offset in the velocities of the intermediate and high velocity Ca II and Na I components in our study. We have been unsuccessful in locating an instrumental or data analysis source for this offset, which leaves open the possibility that the offset is real. In Fig. 5, we present an enlargement of the HD 83206 Ca II spectrum spanning the IVC and HVC at -80 and $-108\,\mathrm{km\,s^{-1}}$, respectively, with single and double compo-

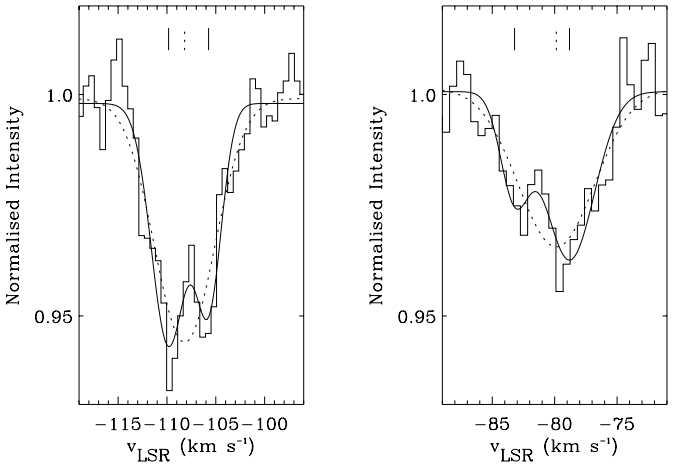

Fig. 5. HD 83206 HVC and IVC Ca II K spectrum at $-110\,\mathrm{km\,s^{-1}}$ and $-80\,\mathrm{km\,s^{-1}}$. Histograms are the observed spectrum. Dotted lines are the fits with one Gaussian component (dotted tick marks show the centroid). Solid lines are the fits with two Gaussian components (solid tick marks show the centroids).

nents fit to the spectra. The profiles are fit slightly better with two components, but at the S/N levels of the data obtained for this star, we are not able to rule out the possibility that the IVC and HVC may be composed of single components. Double component fits yield subcomponents at velocities -109.8, -105.7 and -83.2, -78.8 $\mathrm{km\,s^{-1}}$. Additional observations of this star are needed to study this IVC and HVC structure further.

These new results demonstrate that the cloudlet structure in the IVC towards HD 203664 is not an isolated case. The close proximity of the absorption lines in velocity space (only a few $\mathrm{km\,s^{-1}}$ for most cases) indicates that the cloudlets are related rather than chance coincidences. At the present time, the existing models predicting the origin and evolution of IVCs and HVCs (see below) do not make definitive predictions for the IVC/HVC substructure, and the typical velocity spacing of the cloudlet components. This is partly due to the focus of the current models on making prediction for H I observations, for which it is difficult to resolve the components due to an insufficient sensitivity of H I data and/or blending of the overlapping H I components. However, our results should give additional constraints on modeling the IVCs and HVCs. As these different IVCs/HVC are part of the lower Galactic halo ($z < 2$ kpc), the accretion and fountain models provide explanations for the origin of the HVC with $V_{\mathrm{LSR}} < 200\,\mathrm{km\,s^{-1}}$ (Wakker & van Woerden 1997 and references therein), and should predict precise velocity spacings for the cloudlet components. A systematic study of different sightlines at high resolution and high S/N should be made in order to increase the observational sample, and to determine the prevalence of cloudlet substructure in IVCs/HVCs.

The presence of these cloudlets in the IVCs/HVCs leads to several questions. Why do we observe them? Should these clouds not disperse rather quickly? External and internal conditions may influence the structure seen. For example: (i) Interactions with disk and low halo gases could disrupt and modify the shapes of IVCs/HVCs. Both the accretion and the fountain models could result in direct contact between IVCs/HVCs and disk gases as the IVCs/HVCs fall to the Galactic plane. A simple model of such interactions is given by Benjamin & Danly (1997). (ii) If the cooling time is less than the Jeans time, the cloud will cool rapidly to a temperature T_f, and the gravitational potential will dominate the system causing the cloud to fragment. The cooling time can be defined as $t_c \sim 10^{13}/n_c$ s from Dyson & Hartquist (1983), and the Jeans time is $t_J \sim 4 \times 10^{13}/n_c^{0.5}(T_f/10)^{0.5}$ s (Spitzer 1978), where n_c is the density of the cloudlets, assumed to be of the same order as the density of the non-fragmented IVC/HVC. Thus, at the condition $n_c T_f > 0.6$, the IVC/HVC will fragment, and the fragments will not re-expand. From Spitzer & Fitzpatrick (1993), the density of the cloudlets is 0.02–$0.05\,\mathrm{cm^{-3}}$ along the HD 93521 sightline, which implies a temperature greater than 20 K, to satisfy the fragmentation criterion. Even if this is very schematic, the values obtained agree with H I observations (Wakker & van Woerden 1997 and references therein), and it therefore seems plausible that the cloudlets may not disperse in a short time. This leads to the hypothesis of Dyson & Hartquist (1983), who showed that cloudlet IVC/HVC collisions could account for some of the early-type stars observed in the Galactic halo. With our data it is not possible to conclude that the different cloudlets observed are such sites, but the identification of such cloudlets within a number of IVC and HVC sightlines lends support to the Dyson & Hartquist hypothesis. Recently, Christodoulou et al. (1997) found, using higher resolution H I data than Dyson & Hartquist, that the conditions in the Galactic halo are not favorable for the formation of high mass stars via cloudlet collisions. The principal differences in the models are the core size and velocity dispersions of the clouds used; these were overestimated by Dyson & Hartquist by factors of 10, and 3–10, respectively. However, these simulations are extremely model-dependent, requiring as input detailed information on the sizes, number density, and physical conditions of IVCs and HVCs. All of these parameters are still uncertain (c.f., Wakker & van Woerden 1997).

5. Conclusion

We have presented high resolution and high S/N spectra towards the three Galactic halo stars HD 14633, HD 83206 and HD 93521. Multiple absorption components in the IVCs-HVC gas have been resolved along the different sightlines. The column density ratios suggest that these IVCs and HVC consist of both neutral and shocked gas, and the few $\mathrm{km\,s^{-1}}$ velocity spacing of these different cloudlets imply that they are related. This result demonstrates that the cloudlet structure towards HD 203664 is not unique.

The analysis of these data suggests several areas for further investigation. Additional observation of HD 83206 should be undertaken to confirm the presence of cloudlets in the IVC and HVC along this sightline. More generally, further optical observations at high resolution and high S/N should be undertaken to increase the sample of HVCs, and to see if the cloudlet structure

is common. Also, there is a need for further ultraviolet absorption line observations of IVCs and HVCs in order to model the physical state of the gas. These results should help to constrain existing and future models predicting the origin and evolution of IVCs and HVCs. Models seeking to do so should make definite predictions for the velocity spacing between cloudlets.

Acknowledgements. NL holds a postgraduate studentship from the European Social Fund and Northern Ireland Development for Research. RSIR acknowledges financial support from the UK Particle and Astronomy Research Council. DLL acknowledges the National Science Foundation grant AST9618414 and the Robert A. Welch Foundation of Houston, Texas. This research has made use of the NASA Astrophysics Data System Abstract Service (http://adswww.harvard.edu/) and the CDS database (http://cdsweb.u-strasbg.fr/).

References

Albert C.E., Blades J.C., Morton D.C., et al., 1993, ApJS 88, 81
Benjamin R.A., Danly L., 1997, ApJ 481, 764
Christodoulou D.M., Tohline J.E., Keenan F.P., 1997, ApJ 468, 810
Cram T.R., Giovanelli R., 1976, A&A 48, 39
Dyson J.E., Hartquist T.W., 1983, MNRAS 203, 1233
Hobbs L.M., 1978, ApJS 38, 129
Hobbs L.M., 1983, ApJ 265, 817
Howarth I.D., Murray J., Mills D., Berry D.S., 1996, STARLINK User Note SUN 50, Rutherford Appleton Laboratory/CCLRC
Howarth I.D., Reid A.H.N., 1993, A&A 279, 148
Jenkins E.B., 1996, ApJ 471, 292
Keenan F.P., Shaw C.R., Bates B., Dufton P.L., Kemp S.N., 1995, MNRAS 272, 599
Kuntz K.D., Danly L., 1996, ApJ 457, 703
Lehner N., Dufton P.L., Lambert D.L., Ryans R.S.I., Keenan F.P., 1999, MNRAS submitted
Little J.E., Dufton P.L., Keenan F.P., Conlon E.S., Davies R.D., 1994, ApJ 427, 267
Mihalas D., Binney L., 1981, Galactic Astronomy. 2nd edition, Freeman, San Francisco
Morris R., Privett G., 1995, STARLINK User Note SUN 79, Rutherford Appleton Laboratory/CCLRC
Morton D.C., 1991, ApJS 77, 119
Routly P.M., Spitzer L., 1952, ApJ 115, 227
Ryans R.S.I., Keenan F.P., Sembach K.R., Davies D., 1997a, MNRAS 289, 83
Ryans R.S.I., Keenan F.P., Sembach K.R., Davies D., 1997b, MNRAS 289, 986
Ryans R.S.I., Sembach K.R., Keenan F.P., 1996, A&A 314, 609
Savage B.D., Sembach K.R., 1991, ApJ 379, 245
Sembach K.R., Savage B.D., 1992, ApJS 83, 147
Sembach K.R., Danks A.C., 1994, A&A 289, 539
Spitzer L., 1978, Physical Processes in the Interstellar Medium. Wiley, New York
Spitzer L., Fitzpatrick E.L., 1993, ApJ 409, 299
Stokes G.M., 1978, ApJS 36, 115
Tull R.G., MacQueen P.J., Sneden C., Lambert D.L., 1995, PASP 107, 251
Wakker B.P., Schwarz U.J., 1991, A&A 250, 509
Wakker B.P., van Woerden H., 1997, ARA&A 35, 217
Wallace P.T., Clayton C., 1996, RV, STARLINK User Note SUN 78, Rutherford Appleton Laboratory/CCLRC
Welsh B.Y., Sasseen T., Craig N., Jelinsky S., Albert C.E., 1997, ApJS 112, 507
Welty D.E., Morton D.C., Hobbs L.M., 1996, ApJS 106, 533